

# Coupled-cluster response theory for near-edge x-ray-absorption fine structure of atoms and molecules

Sonia Coriani, Ove Christiansen, Thomas Fransson and Patrick Norman

**Linköping University Post Print**

N.B.: When citing this work, cite the original article.

Original Publication:

Sonia Coriani, Ove Christiansen, Thomas Fransson and Patrick Norman, Coupled-cluster response theory for near-edge x-ray-absorption fine structure of atoms and molecules, 2012, Physical Review A. Atomic, Molecular, and Optical Physics, (85), 2, 022507.

<http://dx.doi.org/10.1103/PhysRevA.85.022507>

Copyright: American Physical Society

<http://www.aps.org/>

Postprint available at: Linköping University Electronic Press

<http://urn.kb.se/resolve?urn=urn:nbn:se:liu:diva-75466>

# Coupled-cluster response theory for near-edge x-ray-absorption fine structure of atoms and molecules

Sonia Coriani

*Department of Chemistry, University of Aarhus, DK-8000 Århus C, Denmark and Dipartimento di Scienze Chimiche e Farmaceutiche, Università degli Studi di Trieste, Via Licio Giorgieri 1, IT-34127 Trieste, Italy*

Ove Christiansen

*Department of Chemistry, University of Aarhus, DK-8000 Århus C, Denmark*

Thomas Fransson and Patrick Norman

*Department of Physics, Chemistry and Biology, Linköping University, SE-581 83 Linköping, Sweden*

(Received 7 September 2011; revised manuscript received 24 November 2011; published 8 February 2012)

Based on an asymmetric Lanczos-chain subspace algorithm, damped coupled cluster linear response functions have been implemented for the hierarchy of coupled cluster (CC) models including CC with single excitations (CCS), CC2, CC with single and double excitations (CCSD), and CCSD with noniterative triple corrected excitation energies CCSDR(3). This work is a first step toward the extension of these theoretical electronic structure methods of well-established high accuracy in UV-vis absorption spectroscopies to applications concerned with x-ray radiation. From the imaginary part of the linear response function, the near  $K$ -edge x-ray absorption spectra of neon, water, and carbon monoxide are determined and compared with experiment. Results at the CCSD level show relative peak intensities in good agreement with experiment with discrepancies in transition energies due to incomplete treatment of electronic relaxation and correlation that amount to 1–2 eV. With inclusion of triple excitations, errors in energetics are less than 0.9 eV and thereby capturing 90%, 95%, and 98% of the relaxation-correlation energies for C, O, and Ne, respectively.

DOI: [10.1103/PhysRevA.85.022507](https://doi.org/10.1103/PhysRevA.85.022507)

PACS number(s): 31.15.A–, 31.15.bw, 31.15.V–, 78.70.Dm

## I. INTRODUCTION

Synchrotron radiation (SR) is an essential ingredient in many scientific areas including physics, chemistry, biology, materials and environmental sciences. It benefits any research area utilizing electromagnetic radiation by providing highly focused, high-intensity light of well-defined characteristics, with wavelengths from the infrared to the x-ray region. Not surprisingly, further development of SR sources is a key strategic measure for scientific excellence, and with the new fourth-generation radiation sources new disciplines and research areas of both fundamental and applied character, like x-ray femtochemistry and dynamic x-ray Raman spectroscopy, will be emerging. Beyond doubt, a concomitant development in theory and simulation technology is called for.

Largely used SR techniques are x-ray absorption spectroscopy (XAS), x-ray circular dichroism (XCD), and x-ray magnetic circular dichroism (XMCD). Multiphoton XAS and XCD experiments are also envisaged in the near future owing to the advances at SR facilities. In all these spectroscopies, the photon energy is tuned to regions of core state resonances, and their successful application relies not only on the development of high quality radiation sources and experimental techniques but also of theoretical methodologies: It is the interplay of experiment and theory that provides a fundamental understanding of the spectra and makes it possible to extract the desired structure information from the measurement. The analysis of the core-level spectra in combination with theoretical calculations discloses detailed electronic and structural information, such as charge-transfer, bonding nature, hybridization, chemical environment, site symmetry, etc. Thus, theoretical simulations are essential

not only to understand specific systems but also to define the information content in the spectroscopic probes. Even though single-particle and atomic-multiplet models [1–5] are routinely employed to interpret XAS spectra, they suffer from inherent limitations. It can therefore be argued that a molecular approach, based on accurate quantum chemical electronic structure methods, is to be preferred, hindered only by the need for methodological development and the computational costs.

The hierarchy of coupled cluster (CC) levels enables a systematic and rapid convergence of dynamic electron correlation, and, with inclusion of triple excitations, very high accuracy for polyatomic molecules (errors of order 0.1 eV) is reached in the description of electronic transitions in the UV-vis region of the spectrum [6,7]. In x-ray spectroscopies, the use of CC response methods is, on the other hand, basically unexplored, hampered mainly by the fact that the semibound core–valence excited states of interest are embedded in a continuum of valence ionized states.

In the present work, we circumvent this issue by a determination of the linear absorption cross section not from the complete oscillator strength distribution (which corresponds to solving fully a large eigenvalue problem) but from the imaginary part of the electric dipole polarizability [8]

$$\sigma(\omega) = \frac{4\pi\omega}{c} \text{Im} [\bar{\alpha}(\omega)], \quad (1)$$

where the overbar denotes the isotropic tensor average. Key to our approach is the taking into account of finite lifetimes of excited states which leads to resonance convergent response functions, also referred to as *damped* response functions, or *complex* polarization propagators [9,10]. A spectrum obtained

with our approach is, in the limit of small spectral broadenings, equivalent to a spectrum composed of individual roots, each broadened by Lorentzian functions. Our calculations of near-edge x-ray absorption fine structure [11] spectra are based on Eq. (1) with the imaginary polarizability obtained from CC linear response functions.

Several quantum mechanical methods are available for the calculation of core-electron excitation spectra, for instance the multiple scattering  $MSX_\alpha$  technique [11], the direct static exchange method STEx [12,13], the transition potential density functional theory (DFT-TP) method [14], the algebraic diagrammatic connection [15] propagator approaches ADC(2) [16] and ADC(3) [17], various methodologies based on time-dependent density-functional theory (TDDFT) [18–21], and the GW/Bethe-Salpeter equation approach [22]. Some of the proposed methods are adapted to specific systems, elements or x-ray adsorption edges, which represents an unphysical dichotomy of methodologies.

Thus, despite the richness of methods available, we argue that the development of a CC ground-state response approach can mark a generation leap through the provision of a clear path toward methods of systematic treatment of core correlation, in combination with the well-known virtues of response theory, such as state orthogonality, size consistency, as well as the extendibility to nonlinear, multiphoton, x-ray phenomena.

Past formulations of CC response theory (see, e.g., Ref. [23]) have been restricted to a calculation of the real-valued, resonance divergent, polarizability and to a “bottom-up” state-by-state determination of excitation energies by solving eigenvalue equations. The damped CC response functions introduced in the present work contain the conventional linear-algebraic building blocks but a different computational strategy is required, and we have here explored a Lanczos chain as the computational vehicle.

It has become increasingly clear that the Lanczos algorithm, a well-known algorithm for solving eigenvalue equations, also has very attractive features as a method to compute certain matrix functions [24] and spectra [25–30]. The algorithm is now exploited in the context of electronic CC theory, where we consider the damped CC response function as a function of the asymmetric characteristic CC response matrix. With an appropriate starting vector, the Lanczos algorithm can be used to calculate spectra simultaneously for all frequencies with well-defined features of global convergence with increasing chain length. The boon here is that this approach emphasizes directly the quantity of interest, that is, the absorption, circumventing the explicit calculation of a great many states that are irrelevant to the formation of the spectrum.

In response theory approaches, the degree to which electronic relaxation effects in core-excited states are retrieved becomes a matter of treatment of electron correlation. Access to the hierarchy of CC approaches enables us to pinpoint the multielectron excited character of this relaxation effect and perform convergence studies with respect to completeness of the cluster expansion. We expect this result to be highly valuable for the benchmarking of more approximate methods such as adiabatic TDDFT that, for core excitations [20,21], are plagued by self-interaction errors [31].

## II. METHODOLOGY

For real reference states, the CC response function for two identical electric-dipole operators can be written as

$$\langle\langle\hat{\mu}_X;\hat{\mu}_X\rangle\rangle_\omega^\gamma = \sum_\mu \eta_\mu^X [t_\mu^X(\omega + i\gamma) + t_\mu^X(-\omega - i\gamma)] + \sum_{\mu\nu} F_{\mu\nu} t_\mu^X(-\omega - i\gamma) t_\nu^X(\omega + i\gamma), \quad (2)$$

with

$$[A - (\omega + i\gamma)\mathbf{1}]t^X(\omega + i\gamma) = -\xi^X \quad (3)$$

and the CC “building blocks”  $\xi_\mu^X$ ,  $\eta_\mu^X$ ,  $F_{\mu\nu}$ , and  $A_{\mu\nu}$  defined in Ref. [23]. We note that the diagonal elements of the polarizability tensor in Eq. (1) equal minus the response function in Eq. (2). This suggests that the solution of complex linear response equations over a grid of input frequencies  $\omega$  and for a given damping parameter  $\gamma$  is required to obtain the absorption spectrum based on Eq. (1). We take a slightly different view and adopt an asymmetric Lanczos-chain algorithm to perform an approximate tridiagonalization of the asymmetric CC Jacobian matrix  $A$ . With  $T$  indicating the tridiagonal representation, we obtain  $T = P^T A Q$ ,  $P^T Q = \mathbf{1}$ , where  $P$  and  $Q$  collect the “Lanczos vectors” generated from the asymmetric Lanczos procedure [32]. As start vectors we use biorthonormal  $\xi^X$  and  $\eta^X$  vectors, that is,

$$q_1 = \frac{\xi^X}{n_\xi}, \quad n_\xi = \|\xi^X\|, \quad (4)$$

$$p_1 = \frac{\eta^X}{n_\eta}, \quad n_\eta = \frac{(\eta^X)^T \xi^X}{n_\xi}, \quad (5)$$

and maintain biorthogonality explicitly throughout, that is,  $p_i^T q_k = \delta_{ik}$ . The nonzero elements of the tridiagonal matrix are computed from the Lanczos vectors as outlined in Ref. [32]. Diagonalization of  $T$ , which is conveniently truncated to dimension  $J \ll n$  ( $n$  being the full dimension), generates an effective spectrum. Formulating the linear response function in terms of the effective spectrum allows for the expedient calculation of Eq. (2) for all frequencies and  $\gamma$  values of interest, according to the following simplified “diagonal” representation,

$$\langle\langle\hat{\mu}_X;\hat{\mu}_X\rangle\rangle_\omega^\gamma = n_\xi n_\eta \sum_j \left\{ \frac{L_{j1} R_{1j}}{(\omega - \omega_j) + i\gamma} - \frac{L_{j1} R_{1j}}{(\omega + \omega_j) + i\gamma} \right\} - n_\xi^2 \sum_{jk} \frac{\mathcal{F}_{kj} L_{j1} L_{k1}}{(\omega - \omega_j + i\gamma)(\omega + \omega_k + i\gamma)}, \quad (6)$$

where the (columns of the) matrix  $R$  and the (rows of the) matrix  $L$  collect, respectively, the right and left eigenvectors of the truncated  $T$  matrix, and  $\mathcal{F}_{kj} = \sum_{\mu\nu} F_{\mu\nu} X_{\mu k} X_{\nu j}$ , with  $X_j = Q R_j$ .

The imaginary component of Eq. (6) used to compute the absorption cross section is easily derived as

$$\begin{aligned} & \text{Im}\langle\langle\hat{\mu}_X;\hat{\mu}_X\rangle\rangle_\omega^\gamma \\ &= \gamma n_\eta n_\xi \sum_j \left\{ \frac{L_{j1} R_{1j}}{(\omega - \omega_j)^2 + \gamma^2} - \frac{L_{j1} R_{1j}}{(\omega + \omega_j)^2 + \gamma^2} \right\} \\ & - \gamma n_\xi^2 \sum_{jk} \frac{\mathcal{F}_{kj} L_{j1} L_{k1} (2\omega + \omega_k - \omega_j)}{[(\omega - \omega_j)^2 + \gamma^2][(\omega + \omega_k)^2 + \gamma^2]}. \quad (7) \end{aligned}$$

Note that in the equations given it is assumed for simplicity that only real eigenvalues are obtained, even though this is not strictly guaranteed due to the non-Hermitian nature of the CC Jacobian. The actual implementation does, however, properly account for the occurrence of complex roots.

Even though Eq. (7) yields the absorption cross-section spectrum straightaway, one may be interested in the oscillator strengths of the individual excitations ( $0 \rightarrow j$ ) contributing to a given band yielded by the Lanczos approach. These are computed straightforwardly, together with the absorption cross section in Eq. (7), from the expression (here given for one dipole-moment Cartesian component  $X$ )

$$f^{XX}(0 \rightarrow j) = \frac{2}{3}\omega_j \left\{ n_\eta n_\xi L_{j1} R_{1j} - n_\xi^2 \sum_l \mathcal{F}_{lj} \frac{L_{j1} L_{l1}}{(\omega_j + \omega_l)} \right\}, \quad (8)$$

obtained as the residue for  $\omega \rightarrow \omega_j$  and  $\gamma = 0$  of the response function in Eq. (6).

Note that with increasing chain length an increasing amount of pseudoeigenvectors will converge to true accurate eigenvectors, allowing standard CC calculations of transition properties. This is a most useful test, but also useful in other ways, such as making noniterative triple excitation corrections using CCSDR(3) possible using those CCSD eigenvectors that can be verified to have converged. Recall still that the essence of the whole strategy is that we do not need to converge all roots explicitly to obtain accurate response functions.

A few comments are in order relative to Eq. (7) and the relation of the damped response theory approach with a standard spectrum obtained by finding eigenvalues and transition properties and subsequently imposing a Lorentzian shape on the individual transitions. For the response function of an exact state there is an exact match between the two (ignoring the contributions from the “emission” term of the response function). For the present approximate CC case there is a close but not formally exact match of the two. We see that the first term in the above CC spectrum equation has exactly the form of a sum of Lorentzians, and discarding the second term is fully equivalent to the steps taken for the exact case. However, the third  $F$ -matrix term formally destroys the exact match as it contains additional dependencies of  $\omega$  and  $\gamma$ . These forms are for example not present if one takes the standard CC response excitation energies and oscillator strengths and imposes a Lorentzian form. The nonvariational structure of CC makes the standard equivalences of exact theory come out slightly different, but it should be remarked that: (i) for the exact untruncated cluster expansion the CC response function matches that of the exact one, and the equivalence is fully retained; (ii) when all equations are fully converged for an approximate wave function, the spectrum will, to a very good approximation, be composed of a sum of Lorentzians since the  $F$ -matrix term represents after all only a minor contribution. Having stated these facts for the purpose of rigor, one can see that in the limit of a complete diagonalization—thus, the Lanczos algorithm has expanded the full matrix—all that our approach has done is essentially to create a Lorentzian convoluted spectrum. In practice, we will neither use exact wave functions nor be able to run the iterative scheme to full resolution of the Jacobian, and it should be emphasized that the

damped response functions enable calculations of absorption without converging the *full* set of eigenvalues and eigenvectors at a given approximation level. The attention then shifts to actually calculating the damped response function, and it is for that purpose that we in this work use the Lanczos algorithm as it has a straightforward path to the full solution (use a long enough chain) and good-enough results in a global sense can be obtained with truncated chains.

For further details on damped CC response theory by a Lanczos driven algorithm, see Refs. [30,33], including in Ref. [30] formal arguments for the specific way the damping is included in the methodology (derived in the context of the closely related vibrational CC response function) and in Ref. [33] algorithmic details in electronic CC theory, with studies of the performance of the approach for a range of different properties. For conciseness we restrain from providing further algorithmic details here and focus instead on specific comments related to understanding the generation of x-ray results before benchmarking the use of CC response methods in XAS.

The use of the iterative, asymmetric, Lanczos algorithm to compute the damped linear response function parallels developments made for the case of molecular vibrational states [28,30], where the density of states in the spectral region of interest is high. The challenge here is similar: We must accurately determine the key contributor to absorption among, in principle, very many other states.

With the present approach we generate the entire absorption spectrum for all frequency values of interest using one common approximate representation of the Jacobian matrix. Thus, we construct by an iterative procedure a tridiagonal matrix (in a reduced space) that is diagonalized once and the approximate spectrum is available according to the above simple equations. Specifically, while the standard bottom-up solution of eigenvalue equations typical to CC response implementations would be impossible to apply for calculating x-ray absorption spectra, the present approach allows us to make access to this spectral region. The Lanczos approach provides effective spectra useful for accurate computations of matrix functions. With the appropriate seed of the Lanczos scheme as given above, the response functions relevant for calculating absorption are converged with increasing precision as the chain length increases. The Lanczos algorithm has attractive convergence features with respect to chain length  $J$ , since higher moments of the spectrum are determined exactly with increasing chain length (see, e.g., Refs. [25,28,30]). The convergence behavior is related to the convergence of the eigenvalues where the Lanczos approach, according to traditional wisdom, converges the extremes before the interior, but the moment perspective also opens for a more global view upon the convergence of absorption, which is needed for our application.

It is here remarkable that the effective Lanczos spectrum generated with emphasis on the calculation of the response function considered as a matrix function, for well-converged spectra has some parts that are converged hard enough to extract useful information on eigenstates. Specifically, we have checked by converting the pseudoeigenvectors  $\mathbf{X}_j$  generated by expanding the eigenvectors of the tridiagonal  $\mathbf{T}$  matrix into the full excitation space whether these may or may not be relative accurate eigenvectors of the CC response Jacobian.

This can be done by using such vectors as start vectors in an ordinary CC response calculation. A typical situation is that the vector that corresponds to the strong absorption feature in the spectrum is also well converged as an eigenvector, while other pseudo-eigenvectors which contributed essentially nothing to the absorption are far from converged. A consequence of this is that we have a way to converge the intense states in the x-ray region. Furthermore, analyzing such states is useful to identify the transitions originating from the core and to determine their percentage of multielectron excited character. The weight of excitations in the response eigenvector is, in fact, one standard way of analyzing the character of the excited states. All states will, due to correlation effects, have a mixture of different excitation levels relative to the Hartree-Fock reference Slater determinant, with typical pure single excitations having around 5%–10% double excitation weight. With much large weight of double excitations (25%–100%) the speed of convergence in the CC hierarchy becomes much slower, which represents another diagnostic of the multielectron excited character of the excited state.

The pseudo-eigenvectors are also used to construct the CCSD eigenvectors needed as restart vectors for the inclusion of triple excitations on the excitation energies via the noniterative CCSDR(3) method [34]. The corrected excitation energies for the peaks giving the absorption are then put back into the pseudo-spectrum with the CCSD transition properties to define a CCSDR(3) spectrum. This pragmatic procedure allows us with noniterative  $N^7$  effort to get the accuracy of triple excitations for the energies without having to suffer full inclusion of triple excitations in all steps of the calculation.

### III. RESULTS

#### A. Computational details

The outlined approach has been implemented in a local version of the DALTON program [35]. All CCS calculations were performed with full excitation space dimension. At the CC2 and CCSD levels, chain lengths of  $J = 3000$ ,  $J = 3000$ , and  $J = 3800$  were used for Ne, H<sub>2</sub>O, and CO, respectively, for each symmetry unique component of the dipole operator (Abelian symmetry only). Symmetry labeling refers to a water molecule placed on the  $YZ$  plane, with the  $C_2$  axis along  $Z$ . Experimental molecular structures are used. Relativistic effects are estimated with use of the second-order Douglas-Kroll-Hess Hamiltonian [36–38].

A common lifetime broadening of  $\gamma = 1000 \text{ cm}^{-1}$  (ca. 0.124 eV) is used, in accordance with previous studies [20,21], which provides a resolution of electronic transitions that exceeds what is found in experimental spectra. Dunning's aug-cc-pCVTZ basis set was adopted for all species [39]. As proposed by Kaufmann and co-workers [40], the original basis sets are supplemented with sets of uncontracted Rydberg functions: for Ne, ( $6s6p$ ) with  $n = 2.5$  to 5 are added and, for H<sub>2</sub>O and CO, ( $3s3p3d$ ) with  $n = 3$  to 4 are placed at the respective center of mass.

#### B. Neon

The accurate experimental NEXAFS spectrum reported by Coreno *et al.* [41] shows a series of three peaks of

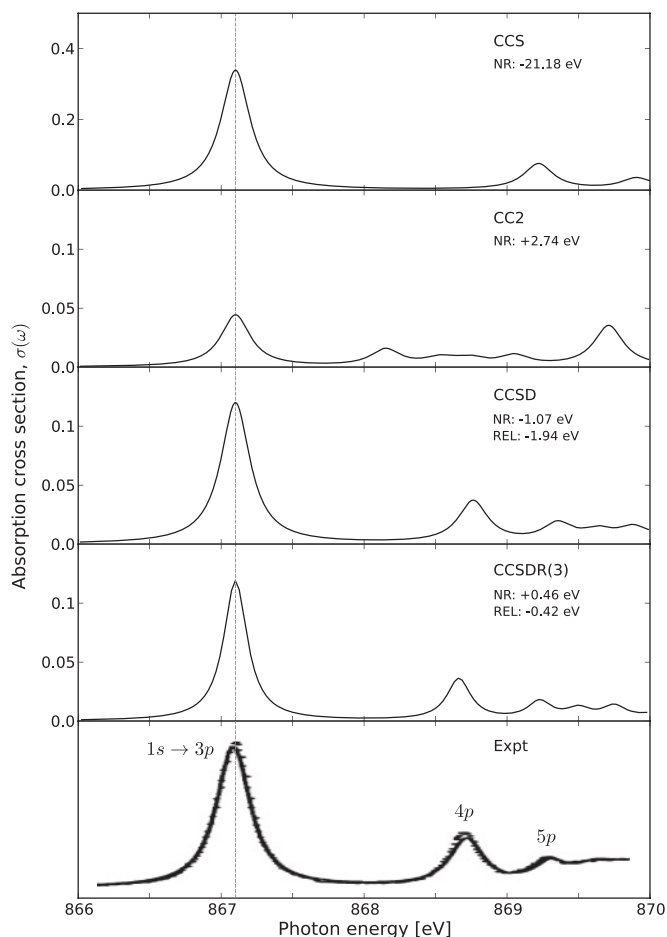


FIG. 1. X-ray absorption spectra for neon as obtained with CC response theory and compared against experiment [41]. The results are aligned against the first given experimental peak, and the corresponding shift is given below the model label for both nonrelativistic (NR) and relativistic (REL) calculations. The NR and REL calculations [CCSD and CCSDR(3)] have the same spectral profile to within the thickness of the line. The theoretical absorption cross section is given in atomic units, whereas arbitrary units are adopted in the case of the experiment.

decreasing intensity centered at 867.12(5), 868.69(4), and 869.27(5) eV, respectively, which are assigned to transitions of the  $1s$  core electron to the  $np$  ( $n = 3, 4, 5$ ) Rydberg orbitals. In Fig. 1, results obtained with the hierarchy of CC approximations are shown together with the experimental spectrum, with an alignment made of the  $1s \rightarrow 3p$  peak for ease of comparison.

The CCS spectrum is ca. 22 eV too high, with far too intense a peak for the  $1s \rightarrow 3p$  transition and incorrect energy separation between the peaks. The CC2 peaks are at about 3 eV lower than the experimental ones, and the energy separations, in particular between the  $n = 3$  and  $n = 4$  peaks, are quite underestimated. The CCSD profile is shifted by about 2 eV, with correct energy separations and relative intensity of the various peaks. Both relativistic and nonrelativistic CCSDR(3) results are within 0.5 eV of the experimental peaks, with the nonrelativistic one underestimating and the relativistic ones overestimating the experimental counterparts. The transitions have approximately 10% of double excitation character.

TABLE I. Compilation of excitation energies  $\omega_j$  (eV) and oscillator strengths  $f$  of selected core excitations (vertical transitions) as obtained from the Lanczos procedure. Label NR stands for nonrelativistic, REL for relativistic results (via the Douglas-Kroll-Hess Hamiltonian).

Excitation	$\omega_j$	$f$	Method
Ne( $1s \rightarrow 3p$ )	866.64	0.01187	CCSDR(3)-NR
	868.17	0.01187	CCSD-NR
	864.36	0.00435	CC2-NR
	888.28	0.03366	CCS-NR
	867.52	0.01189	CCSDR(3)-REL
	869.06	0.01189	CCSD-REL
Ne( $1s \rightarrow 4p$ )	868.20	0.00350	CCSDR(3)-NR
	869.84	0.00350	CCSD-NR
	865.41	0.00140	CC2-NR
	890.39	0.00721	CCS-NR
	869.08	0.00351	CCSDR(3)-REL
	870.72	0.00351	CCSD-REL
Ne( $1s \rightarrow 5p$ )	868.77	0.00151	CCSDR(3)-NR
	870.42	0.00151	CCSD-NR
	865.79	0.00061	CC2-NR
	891.07	0.00287	CCS-NR
	869.65	0.00151	CCSDR(3)-REL
	871.31	0.00151	CCSD-REL
Ne( $1s \rightarrow 6p$ )	869.04	0.00086	CCSDR(3)-NR
	870.71	0.00086	CCSD-NR
	865.99	0.00061	CC2-NR
	891.39	0.00150	CCS-NR
	869.91	0.00084	CCSDR(3)-REL
	871.59	0.00084	CCSD-REL
H <sub>2</sub> O( $O_{1s} \rightarrow 3s$ )	534.54	0.0128	CCSDR(3)-NR
	535.68	0.0128	CCSD-NR
	534.34	0.0067	CC2-NR
	551.23	0.0409	CCS-NR
	534.87	0.0129	CCSDR(3)-REL
	536.02	0.0129	CCSD-REL
H <sub>2</sub> O( $O_{1s} \rightarrow 3p$ )	536.36	0.0262	CCSDR(3)-NR
	537.47	0.0262	CCSD-NR
	535.88	0.0085	CC2-NR
	551.88	0.0758	CCS-NR
	536.70	0.0262	CCSDR(3)-REL
	537.81	0.0262	CCSD-REL
CO( $C_{1s} \rightarrow \pi^*$ )	287.97	0.1656	CCSDR(3)-NR
	288.21	0.1656	CCSD-NR
	289.55	0.1755	CC2-NR
	294.41	0.2624	CCS-NR
	288.05	0.1653	CCSDR(3)-REL
	288.31	0.1653	CCSD-REL
CO( $O_{1s} \rightarrow \pi^*$ )	534.50	0.0813	CCSDR(3)-NR
	535.85	0.0813	CCSD-NR
	535.41	0.0726	CC2-NR
	550.09	0.1393	CCS-NR
	534.97	0.0816	CCSDR(3)-REL
	536.18	0.0816	CCSD-REL

For future reference we also report in Table I individual values of the vertical excitation energies and corresponding oscillator strengths  $f$  [the latter computed according to

Eq. (8)] for the first four transitions from the core. To generate the CCSDR(3) spectrum, CCSDR(3) excitation energies—obtained restarting the CCSDR(3) calculation from the CCSD pseudo-eigenvectors—and CCSD oscillator strengths have been used, along with a Lorentzian line-shape convolution function.

### C. Water

The experimental  $K$ -edge photoabsorption spectrum recorded by Schirmer *et al.* [42] is characterized by five distinct peaks in the region 533–540 eV (vibrational states are not resolved). The first two peaks (534.0 and 535.9 eV) are assigned to individual states of  $A_1$  and  $B_2$  symmetry, respectively, whereas the remaining three peaks represent convolutions of excitations to the virtual orbitals  $4a_1$ ,  $2b_1$ , and  $2b_2$ . The intensity of the peaks depends on the local  $p$  character of the empty orbitals at the oxygen nucleus.

Figure 2 shows the theoretical spectra together with the experimental spectrum [42], and the theoretical spectra are shifted as to align the first peak to the corresponding experimental peak. For completeness, Table I also reports individual

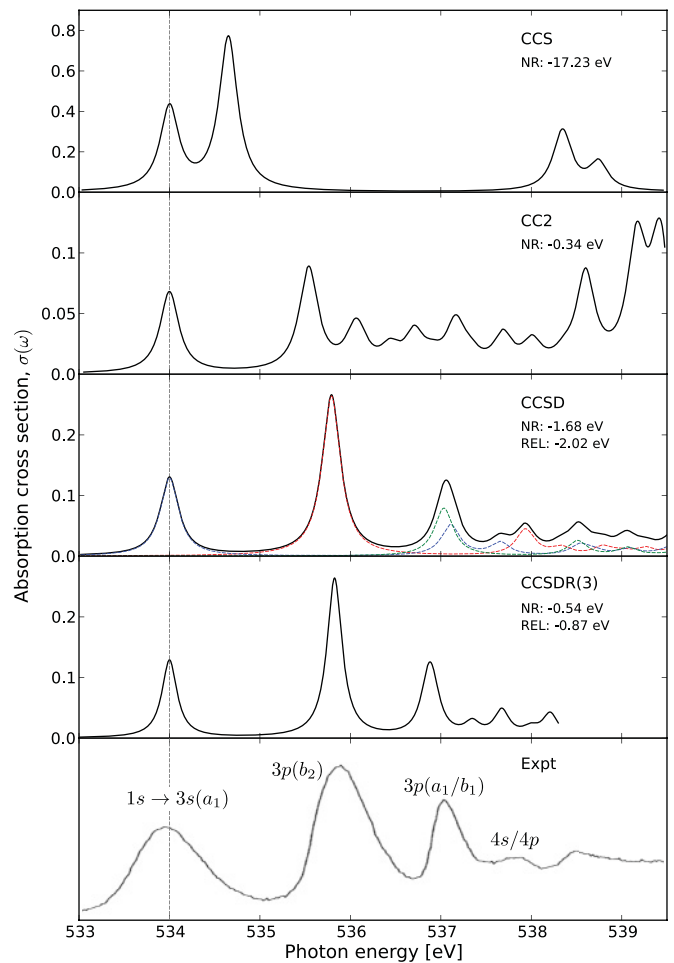


FIG. 2. (Color online) X-ray absorption spectra for water as obtained with CC response theory and compared against experiment [42]. The contribution from the different components of the dipole operator are indicated for the CCSD spectrum. For other details, see caption of Fig. 1.

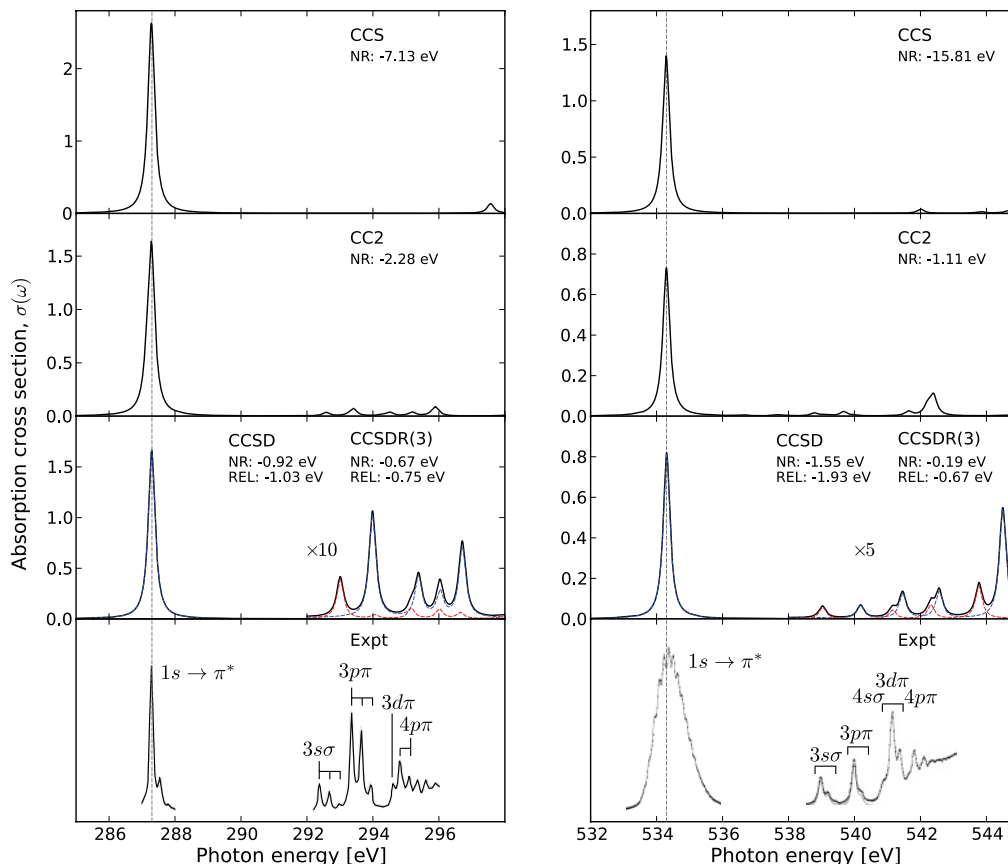


FIG. 3. (Color online) X-ray absorption spectra for carbon monoxide as obtained with CC response theory and compared against experiment [43,44]. The contribution from the different components of the dipole operator are indicated for the CCSD spectrum. For other details, see caption of Fig. 1.

excitation energies and oscillator strengths of the first two core transitions. As can be observed, the CCS spectrum strongly overestimates transition energies and yields incorrect peak separations. CC2 greatly improves on transition energies but provides poor peak separations. At the CCSD level, peak separations are within 0.1 eV of the experimental results and relative peak intensities are in good agreement with experiment. Inclusion of triple excitations and relativistic effects brings the theoretical results for absolute transition energies to within 0.9 eV. For comparison, in a recent study using the complex polarization propagator approach for the density functionals LB94 and CAM-B3LYP and the taug-cc-pVDZ basis, Ekström *et al.* [20,21] obtained spectra qualitatively similar to ours, but with relative shifts of as much as 4.0 eV (LB94) and 15.15 eV (CAM-B3LYP). Moreover, limiting ourselves to the first two excitations, our nonrelativistic results are 534.54 eV for the vertical excitation energy of the  $4a_1$  transition, with an oscillator strength  $f$  of 1.28, and 536.36 eV ( $f = 2.62$ ) for the  $2b_2$  transition. The corresponding ADC(2) results [42] are 532.76 eV ( $f = 0.944$ ), and 534.71 ( $f = 1.83$ ).

We note that the double-excitation character of the transitions is on the order of 10%–15%.

#### D. Carbon monoxide

The dominant spectral feature at both the oxygen and carbon  $K$ -edges is given by the  $1s \rightarrow \pi^*$  band positioned

at 287.4 eV [43] and 534.2 eV [44], respectively. It is followed by a sequence of much weaker discrete bands associated to Rydberg transitions: first, the  $1s \rightarrow 3s\sigma$  band at about 292.4 eV (C) and 539 eV (O) and second, the  $1s \rightarrow 3p\pi$  band at 293.3 eV (C) and 540 eV (O). A series of high-resolution experiments [16,43–47] have clarified the vibrational progressions of such transitions, but this aspect is beyond the scope of the present work.

The theoretical results shown in Fig. 3 reproduce the discussed experimental spectral profiles at both edges; see also Table I for individual energies and strengths of the first core excitation. Neglecting presumably small vibrational corrections, the difference between the energies found from the essentially uncorrelated CCS level of theory and those found in experiment gives an approximate measure of the relaxation and correlation effects that are here treated together as a correlation problem. Focusing first on the main  $\pi^*$  bands, we see that the relaxation-correlation energies amount to 7.1 and 15.8 eV at the carbon and oxygen  $K$  edges, respectively. At the highest level of theory, CCSDR(3) with inclusion of relativistic effects, about 90% and 95% of the relaxation-correlation contribution is captured for C and O, respectively. Analysis of the pseudoeigenvectors for the two intense  $1s \rightarrow \pi^*$  transitions indicates 9% double-excitation character at the carbon  $K$  edge and around 12% double-excitation character at the oxygen  $K$  edge. At the relativistic CCSD level, the oscillator

strengths of the intense transitions are 0.1653 (carbon edge) and 0.0816 (oxygen edge), and they compare well with the corresponding experimentally derived values of 0.167 [48] and 0.06 [49]. Note that, for the  $C_{1s} \rightarrow \pi^*$  band, Triguero *et al.* [14] reported, using the DFT-TP method, nonrelativistic results for the excitation energies between 287.5 and 288.9 eV, with oscillator strengths between 0.162 and 0.164, depending on the functional adopted. With a revised ADC(2) approach in combination with the core-valence separation (CVS) approximation, Trofimov *et al.* [16] obtained a nonrelativistic value of 287.15 eV and an oscillator strength of 0.145. Within the electron-attachment equation-of-motion (EA-EOM) CCSD method, Nooijen and Bartlett [50] calculated 287.52 eV and 0.169 using a closed-shell variant based on the neutral ground-state orbitals (called QRHF/EA-EOMCCSD) and 287.08 eV ( $f = 0.190$ ) with the open-shell variant. Our corresponding nonrelativistic CCSDR(3)/CCSD results are 287.97 eV and 0.1656. For the  $O_{1s} \rightarrow \pi^*$  transition, we calculate 534.49 eV and 0.0813, whereas the DFT-TP [14] results are between 535.1 and 536.1 eV ( $f = 0.066$ ), ADC(2) yields 532.53 eV and 0.07 [16], the QRHF/EA-EOMCCSD method [50] gives 533.98 eV and 0.031, and its open-shell variant [50] yields 534.15 eV and 0.083. Similar to water, using the CPP approach at the TDDFT level, Ekström *et al.* [20,21] reported an absorption spectrum for the C edge qualitatively consistent with the experimental spectrum, but with shifts of as much as +4.8 eV (LB94) and +14.8 eV (CAM-B3LYP) and weaker intensity.

Intensities in the Rydberg regions are much weaker as compared to the  $\pi^*$  bands, and, for clarity, the CCSDR(3) spectra for carbon and oxygen are magnified by factors of 10 and 5, respectively. We note that our calculation correctly captures the  $3s\sigma$  and  $3p\pi$  transitions, which are about equally intense at the oxygen  $K$  edge but not so at the carbon  $K$  edge, where the  $3p\pi$  peak strongly dominates. The polarization dependence of the absorption is depicted in Fig. 3 by the dashed curves, and, upon closer inspection of the carbon spectrum, it is clear that our results support the identification of a  $3p\sigma$  progression under the  $3p\pi$  one (as suggested by Domke [45]). Also in the carbon spectrum, the polarization dependence clearly reveals the  $3d\pi$  shoulder to the left of the  $4p\pi$  band, and, for oxygen, we note the  $4s\sigma$  shoulder (relevant polarization is plotted in red (lighter gray)) to the left of the  $3d\pi/4p\pi$  bands.

#### IV. CONCLUDING REMARKS

We have presented a formulation and implementation of the complex polarization propagator for the hierarchy of

CC response methods CCS, CC2, and CCSD based on an asymmetric Lanczos algorithm and with triple excitation effects on the energetics accounted for using the CCSDR(3) approximation. This hierarchy of theoretical levels provides a generic and systematic way to treat multielectron excitations (shake-up processes) as well as a way to account for electronic relaxation effects. The approach has been applied to the calculation of near  $K$ -edge x-ray absorption spectra of Ne,  $H_2O$ , and CO, thereby illustrating the applicability of standard CC response methods to x-ray spectroscopies. The accuracy of the description of electronic relaxation and differential correlation for the core-excited state depends only on the accuracy in the description of dynamic electron correlation, and it can be monitored by using the CC hierarchy, as typically done for UV-vis spectra. The multielectron excited character that accounts for the relaxation effect amounts to about 10%–15% for the studied transitions at the  $K$  edges. In terms of peak separation energies and intensities, the agreement between CCSDR(3) and experimental spectra is excellent. In absolute terms, the CCSDR(3) energies (with relativistic corrections) are on the order 0.4–0.9 eV too high. The remaining effects are anticipated to be due to a subtle combination of remaining basis set and correlation errors as well as vibrational effects for the molecules. While in absolute terms these energy discrepancies are about five times larger than what is reported in the UV-vis region, the agreement is, in a relative sense, significantly better. This work should be seen in view of the importance of CC response methods for UV-vis spectroscopies, and there is reason to believe that CC response calculations can become the standard benchmark also in the x-ray region. Obviously, the present theoretical methods can be extended to higher-level CC methods giving higher accuracy at higher cost. Another interesting future perspective is that the combination of CC with molecular mechanics methods opens for calculations of much larger systems, where accuracy can still be maintained for a specific central core region.

#### ACKNOWLEDGMENTS

The authors acknowledge discussions with Professor H. Ågren, Professor P. Decleva, Professor H. J. Aa. Jensen, and Professor J. Olsen; financial support from the EU (FP7-PEOPLE-2009-IEF, Project No. 254326) and the Swedish Research Council (Grant No. 621-2010-5014); and a grant for computing time at the National Supercomputer Centre (NSC), Sweden.

- [1] J. J. Rehr and R. C. Albers, *Rev. Mod. Phys.* **72**, 621 (2000).
- [2] J. J. Rehr and A. L. Ankudinov, *J. Synchrotron Radiat.* **8**, 61 (2001).
- [3] J. J. Rehr and A. L. Ankudinov, *J. Synchrotron Radiat.* **10**, 43 (2003).
- [4] F. de Groot, *Chem. Rev.* **101**, 1779 (2001).
- [5] J. J. Rehr, J. J. Kas, M. P. Prange, A. P. Sorini, Y. Takimoto, and F. Vila, *C. R. Phys.* **10**, 548 (2009).
- [6] O. Christiansen, J. Gauss, J. F. Stanton, and P. Jørgensen, *J. Chem. Phys.* **111**, 525 (1999).

- [7] M. R. Silva-Junior, S. P. A. Sauer, M. Schreiber, and W. Thiel, *Mol. Phys.* **108**, 453 (2010).
- [8] R. W. Boyd, *Nonlinear Optics*, 3rd ed. (Academic Press, San Diego, 2008).
- [9] P. Norman, D. M. Bishop, H. J. Aa. Jensen, and J. Oddershede, *J. Chem. Phys.* **115**, 10323 (2001).
- [10] P. Norman, D. M. Bishop, H. J. Aa. Jensen, and J. Oddershede, *J. Chem. Phys.* **123**, 194103 (2005).
- [11] J. Stöhr, *NEXAFS Spectroscopy* (Springer, Berlin, 1992).

- [12] H. Ågren, V. Carravetta, O. Vahtras, and L. G. M. Pettersson, *Chem. Phys. Lett.* **222**, 75 (1994).
- [13] U. Ekström, P. Norman, and V. Carravetta, *Phys. Rev. A* **73**, 022501 (2006).
- [14] L. Triguero, L. G. M. Pettersson, and H. Ågren, *Phys. Rev. B* **58**, 8097 (1998).
- [15] J. Schirmer, *Phys. Rev. A* **26**(5), 2395 (1982).
- [16] A. B. Trofimov, T. E. Moskovskaya, E. V. Gromov, N. M. Vitkovskaya, and J. Schirmer, *J. Struct. Chem.* **41**, 483 (2000).
- [17] A. B. Trofimov, G. Stelter, and J. Schirmer, *J. Chem. Phys.* **111**, 9982 (1999).
- [18] N. A. Besley and F. A. Asmuruf, *Phys. Chem. Chem. Phys.* **12**, 12024 (2010).
- [19] M. Stener, G. Fronzoni, and M. de Simone, *Chem. Phys. Lett.* **373**, 115 (2003).
- [20] U. Ekström, P. Norman, V. Carravetta, and H. Ågren, *Phys. Rev. Lett.* **97**, 143001 (2006).
- [21] U. Ekström and P. Norman, *Phys. Rev. A* **74**, 042722 (2006).
- [22] J. Vinson, J. J. Rehr, J. J. Kas, and E. L. Shirley, *Phys. Rev. B* **83**(11), 115106 (2011).
- [23] O. Christiansen, P. Jørgensen, and C. Hättig, *Int. J. Quantum Chem.* **68**, 1 (1998).
- [24] G. H. Golub and G. Meurant, *Matrices, Moments and Quadratures with Applications* (Princeton University Press, Princeton and Oxford, 2010).
- [25] H. D. Meyer and S. Pal, *J. Chem. Phys.* **91**, 6195 (1989).
- [26] W. C. Haxton, K. M. Nolle, and K. M. Zurek, *Phys. Rev. C* **72**, 065501 (2005).
- [27] D. Rocca, R. Gebauer, Y. Saad, and S. Baroni, *J. Chem. Phys.* **128**, 154105 (2008).
- [28] P. Seidler, M. B. Hansen, W. Gyroffly, D. Toffoli, and O. Christiansen, *J. Chem. Phys.* **132**, 164105 (2010).
- [29] S. Kopelke, K. Gokhberg, L. S. Cederbaum, F. Tarantelli, and V. Averbukh, *J. Chem. Phys.* **134**, 024106 (2011).
- [30] B. Thomsen, M. B. Hansen, P. Seidler, and O. Christiansen, *J. Chem. Phys.* (reviewers' indication "accept with minor revision").
- [31] G. Tu, Z. Rinkevicius, O. Vahtras, H. Ågren, U. Ekström, P. Norman, and V. Carravetta, *Phys. Rev. A* **76**, 022506 (2007).
- [32] G. H. Golub and C. F. van Loan, *Matrix Computations*, 2nd ed. (The Johns Hopkins University Press, Baltimore and London, 1989).
- [33] S. Coriani, O. Christiansen, T. Fransson, and P. Norman, *J. Chem. Theory and Comput.* (reviewers' indication "accept with minor revision").
- [34] O. Christiansen, H. Koch, and P. Jørgensen, *J. Chem. Phys.* **105**, 1451 (1996).
- [35] DALTON, a *Molecular Electronic Structure Program* (2011), Release Dalton 2011; see [<http://daltonprogram.org/>].
- [36] M. Douglas and N. M. Kroll, *Ann. Phys. (New York)* **82**, 89 (1974).
- [37] G. Jansen and B. A. Hess, *Phys. Rev. A* **39**, 6016 (1989).
- [38] P. Norman, B. Schimmelpfennig, K. Ruud, H. J. A. Jensen, and H. Ågren, *J. Chem. Phys.* **116**, 6914 (2002).
- [39] D. E. Woon and T. H. Dunning, *J. Chem. Phys.* **103**, 4572 (1995).
- [40] K. Kaufmann, W. Baumeister, and M. Jungen, *J. Phys. B* **22**, 2223 (1989).
- [41] M. Coreno, L. Avaldi, R. Camilloni, K. C. Prince, M. de Simone, J. Karvonen, R. Colle, and S. Simonucci, *Phys. Rev. A* **59**, 2494 (1999).
- [42] J. Schirmer, A. B. Trofimov, K. J. Randall, J. Feldhaus, A. M. Bradshaw, Y. Ma, C. T. Chen, and F. Sette, *Phys. Rev. A* **47**, 1136 (1993).
- [43] Y. Ma, C. T. Chen, G. Meigs, K. Randall, and F. Sette, *Phys. Rev. A* **44**, 1848 (1991).
- [44] R. Püttner, I. Dominguez, T. J. Morgan, C. Cisneros, R. F. Fink, E. Rotenberg, T. Warwick, M. Domke, G. Kaindl, and A. S. Schlachter, *Phys. Rev. A* **59**, 3415 (1999).
- [45] M. Domke, C. Xue, A. Puschmann, T. Mandel, E. Hudson, D. A. Shirley, and G. Kaindl, *Chem. Phys. Lett.* **173**, 122 (1990); **174**, 668(E) (1990).
- [46] K. C. Prince, M. Vondracek, J. Karvonen, M. Coreno, R. Camilloni, L. Avaldi, and M. de Simone, *J. Electron Spectrosc. Relat. Phenom.* **103**, 141 (1999).
- [47] M. Coreno, M. de Simone, K. C. Prince, R. Richter, M. Vondracek, L. Avaldi, and R. Camilloni, *Chem. Phys. Lett.* **306**, 269 (1999).
- [48] R. B. Kay, Ph. E. van der Leeuw, and M. J. van der Wiel, *J. Phys. B* **10**, 2513 (1977).
- [49] E. Rühl and A. P. Hitchcock, *J. Am. Chem. Soc.* **111**, 2614 (1989).
- [50] M. Nooijen and R. J. Bartlett, *J. Chem. Phys.* **102**, 6735 (1995).